Performance Assessment of a Photovoltaic-Thermal Roof with Modular Heat Exchanger

Steffen Brötje[1], Maik Kirchner[1], Thomas Schabbach[2] and Federico Giovannetti[1]

[1] Institute for Solar Energy Research GmbH Hamelin (ISFH), Am Ohrberg 1, 31860 Emmerthal

Tel.: +495151/999-501; E-Mail: giovannetti@isfh.de

[2] Hochschule Nordhausen, Institut für Regenerative Energietechnik, Weinberghof 4, 99734 Nordhausen

Abstract

This paper presents the thermal performance of a novel photovoltaic-thermal (PV/T) system conceived for roof integration. The methods of prototype design are described briefly. Main feature of the system is the modular assembly of the metallic heat exchanger, which also serves as self-supporting mounting device for the photovoltaic modules and assumes a static function. The design of the heat exchanger has been optimized by using numerical FEM simulations with regard to both energetic and economic requirements. We investigate the performance of the system by means of long-term measurements on a large-sized PV/T roof prototype equipped with thin film CdTe photovoltaic modules under real weather conditions and at different operation conditions. The evaluation is carried out according to the Standard ISO 9806, focusing on the quasi-dynamic test method. The experimental results ($\eta_{0,\,MPP}$ = 0.66; a_1 = 11.56 W/m²K; a_2 = 0.09 W/m²K²; a_3 = 1.26 J/(m³K), a_6 = 0.03 s/m) prove the efficient heat transfer from the absorber to the fluid and are in good agreement with the simulations.

Keywords: photovoltaic-thermal collector, building integration, quasi-dynamic test method

Nomenclature

A_{coll}	PVT collector gross area
b_1	Heat loss coefficient (uncovered collector ISO 9806:2013) at (ϑ_m - ϑ_a) = 0 (W/(m²·K))
b_2	Wind dependence of the heat loss coefficient (uncovered collector ISO 9806:2013) (Ws/(m³·K))
b_u	Collector efficiency coefficient (wind dependence) (uncovered collector ISO 9806:2013) (s/m)
a_1	Heat loss coefficient at (ϑ_m - ϑ_a) = 0 (quasi dynamic model) (W/(m²·K))
a_2	Temperature dependence of the heat loss coefficient (quasi dynamic model) (W/(m²·K²))
a_3	Wind speed dependence of the heat loss coefficient (quasi dynamic model) (J/(m³·K))
a_4	Sky temperature dependence of the heat loss coefficient (quasi dynamic model)
a_5	Effective thermal capacity (J/(m²·K))
a_6	Wind dependence in the zero loss efficiency (quasi dynamic model) (s/m)
a_7	Wind speed dependence of IR radiation exchange a_4 (W/(m²·K⁴))
a_8	Radiation losses (W/(m²·K⁴))
G"	Net irradiance according to ISO 9806:2013 (W/m²)
G_b, G_{hem}	Hemispherical solar irradiance, direct solar irradiance (W/m²)
K_b	Incident angle modifiers (IAM) for direct irradiance
K_d	Incidence angle modifier for diffuse irradiance
$\dot{Q}_{th}$	Useful heat flow (W)
s_{eq}	Thickness of air layer equivalent (mm)
T_a, ϑ_a	Ambient Temperature (K, °C)
$T_{Cell,m}$	Determined cell temperatures in FEM model (K, °C)
$T_{f,m}$, ϑ_m	Mean fluid (heat carrier) temperature (K, °C)
U	Wind speed (m/s)
U_{int}	Internal heat transfer coefficient between solar cells and heat carrier (W/(m²·K))
U_L	Heat loss coefficient at (ϑ_m - ϑ_a) = 0 (W/(m²·K))
Y	Temperature power coefficient of the PV module (%/100)
A	Thermal absorption coefficient of the PV module (measured)
E	Thermal emissivity of the PV module
$\eta_{0,b}$	Conversion factor (thermal efficiency at (ϑ_m - ϑ_a) = 0) for direct incident radiation
$\eta_{0,hem}$	Conversion factor (thermal efficiency at (ϑ_m - ϑ_a) = 0) for hemispherical radiation
η_{el}	Electrical efficiency of the PV module under standard test conditions (STC)

1. Introduction

Photovoltaic-thermal (PV/T) devices convert solar radiation into both useful heat and electricity. This paper shows the design optimization and analyses the thermal and electrical performance of a specific uncovered system for roof-integration comprising a particularly slender and uniform architectural appearance. Other solutions exist on the market, most of them intended for on-roof installation (Brötje et al., 2018). For solar heat production, a heat exchanger has been assembled to the rear side of the modules. The geometry of the heat exchanger was improved, which led to the prototypic solution shown in Figure 1: Planar aluminium profiles with

Selection and/or peer review under responsibility of Scientific Committee
doi:10.18086/eurosun2018.02.10 Available at http://proceedings.ises.org

integrated fluid channels which serve both as mounting system for the PV modules and for the heat carrier transport. Design targets of this device were efficient heat transfer and easy on-roof assembly likewise. The PV modules are clamped onto the aluminium profiles without use of adhesive layers. The design approach improves the architectural appearance of the overall system, as the profiles can be integrated into the roof construction. The design is modular to allow tight adaption to many standard roof dimensions and geometries. This also reduces convective heat losses; apart from tight roof integration, the heat exchanger is not further insulated against the ambience. Hence, the system is designed for low-temperature heat production that generally require heat pump applications to supply space heating or domestic hot water systems.

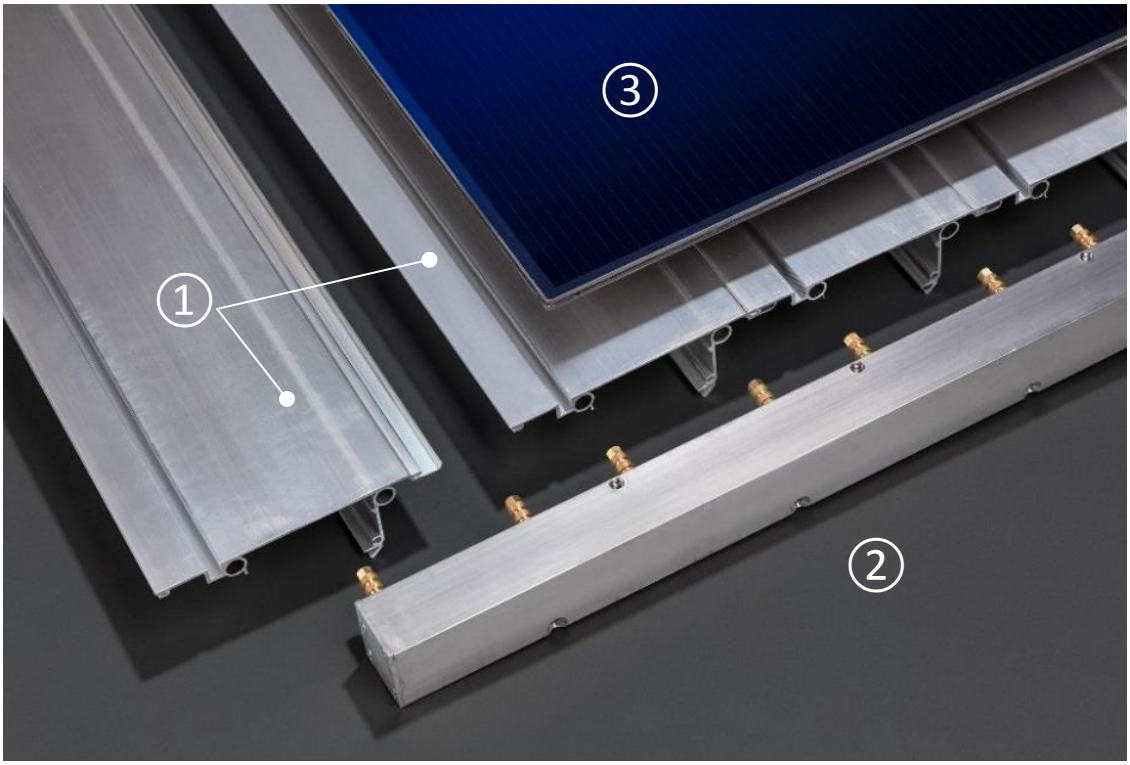

Figure 1: (Unassembled) main components of the PV/T system: Extruded profiles ①, manifold ② and PV module ③.

During the design process that led to the prototype shown in Figure 1, the overall heat transfer was analysed and optimized by means of finite-element-method (FEM) modelling of the heat transfer and hydraulic resistance modelling. The methods used for evaluating the heat transfer and the energy efficiency are mainly based on previous research works, measurements and numerical calculations referring to the potential of PV/T collectors with glue-free and detachable connections of PV module and heat exchanger, as described in Brötje et al. (2018). We proceed to refer the final design stage of this process in section 2 and report experimental tests obtained with the established prototype in section 3. The prototype was tested at the outdoor test facility of the Institute of Solar Energy Research (ISFH).

2. Prototype design

2.1 Preliminary developments

Before developing the PV/T system presented here, the manufacturers of the new system developed a predecessor PV/T system. That system built upon an existing roof-integrated cadmium-telluride based PV system by the same manufacturer. Using the same outdoor test environment as in the following investigations, the previous PV/T system showed a thermal zero-loss efficiency of $\eta_{0,hem}$ = 44 % in open-circuit (OC) operation of the PV generator. Due to the construction, which included loose connections of heat exchanger and fluid pipes as well as profiled, partly curved surfaces, critical heat resistances were detected during testing. These were identified and quantified by a combined simulation/measurements approach. This enabled us to draw conclusions for the new system by means of efficiency and costs. Comparative performance tests on several other PV/T prototypes developed at ISFH have proven a high performance level of the new system, even with clamped and glue-free compound and glass-glass modules. It turned out that the most important design requirement is a flat surface of the extruded aluminium profile (Brötje et al., 2018).

2.2 Heat transfer modelling and optimisation

The heat transfer properties of the PV/T prototype were optimized by means of finite element method (FEM) modelling & simulation using the software suite *Comsol Multiphysics 4.4*. The simulation studies concerned variations of the design geometry, material selections, and also variations of manufacturing tolerances (irregularities, macroscopic unevenness and surface roughness of the heat exchanger) that may lead to misconnections between heat exchanger and PV module. Inherent side conditions of the thermal optimization routine were mechanical stability of the device as well as minimal manufacturing effort of the assembly parts (components and hydraulic connections). The following aspects have been considered during the modelling:

- Distance between fluid channels of the heat exchanger profile / number of channels per profile
- Material strengths of heat exchanger profile, PV glass and possible connecting materials
- Special geometries related to the roof integration, such as the distance between heat exchanger upper surface and fluid channels
- Heat resistances between PV module and heat exchanger surface, expressed as equivalent air gap s_{eq}
- Optical properties of heat exchanger coating (e.g. anti-corrosive)
- Type and concentration of heat carriers, such as water and mixtures of water and ethylene glycol or propylene glycol
- Mass flow rate of the heat carrier, correlating with number of fluid channels and channel diameter.

We employ the overall internal heat transfer coefficient U_{int} as appropriate target quantity for the thermal optimization procedure. It is defined by

$$U_{\mathrm{int}} = \frac{\dot{Q}_{\mathrm{th}}}{A_{\mathrm{coll}} \cdot (T_{\mathrm{Cell,m}} - T_{\mathrm{f,m}})}, \qquad (1)$$

where $\dot{Q}_{\mathrm{th}}$ denotes the useful heat flow, A_{coll} the PVT collector gross area, $T_{\mathrm{Cell,m}}$ the simulated mean PV module temperatures and $T_{\mathrm{f,m}}$ the mean temperature of the heat carrier fluid, respectively.

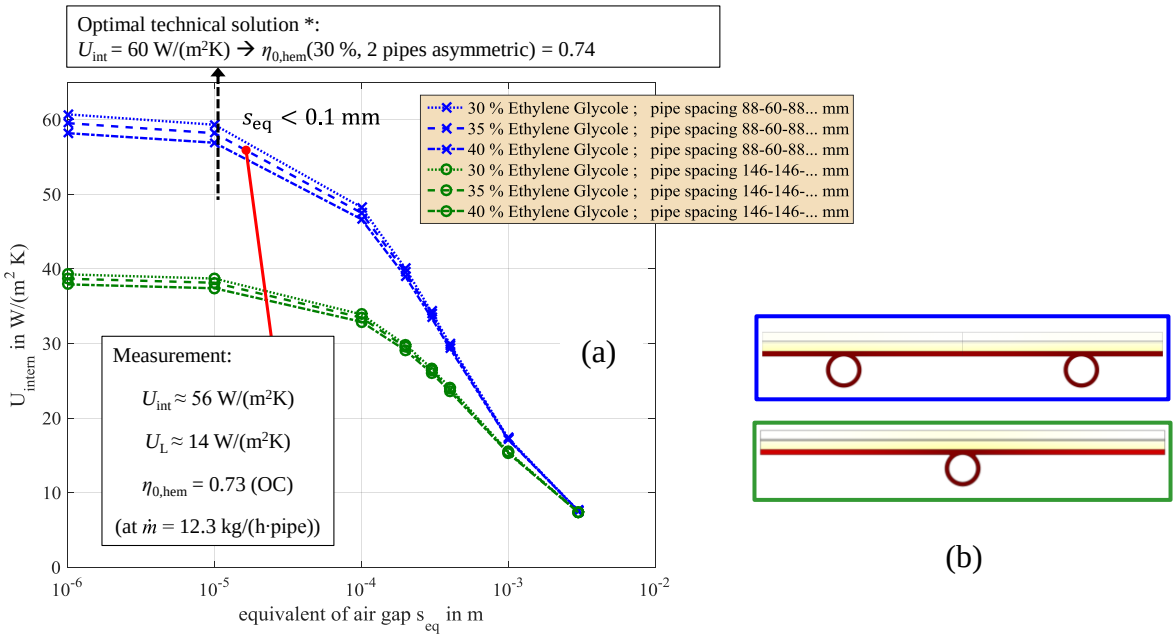

Figure 2: (a) Simulations of the internal heat transfer coefficient U_{int} compared to the value resulted from the measurement of the PV/T prototype test field. *: 2 sheets Al-Al at 1 bar, according to: (Incropera et al., 2002). (b) Cross-sectional sketches of the final design solutions (pipe separations 88-60-88 mm and 146-146 mm per fin. The asymmetric spacing of the channels of the former results from structural conditions of the mounting system.

Manufacturing irregularities, macroscopic unevenness and surface roughness of the heat exchanger can impair the thermal contact between heat exchanger and PV module. Such misconnections are represented by a homogeneous air gap with variable width s_{eq} across the collector area in the FEM model. Hence, the modelled heat resistance becomes a function of the width variable s_{eq}, which in turn can be fitted to the measured data of the prototype. Smaller values of s_{eq} correspond to reduced assembly part misconnections and improve the internal heat transfer coefficient. Reduced misconnections can be achieved through higher manufacturing

quality, however at the expense of increased manufacturing costs. Since U_{int} is also dependent of other design options like the distance of the fluid channels or the material choice, a remnant small value of s_{eq} may be tolerated. (Brötje et al., 2018). Figure 2(a) shows the relation of the internal heat transfer coefficients U_{int} and the equivalent air gap s_{eq} for two different designs (88-60-88 mm and 146-146 mm pipe distance, respectively, see (b)) and different glycole concentrations of the heat carrier fluid. The fluid channels are modelled as parallel pipes for the sake of simplicity, which are part of the mounting plate fins at the given separations. Other pipe configurations have been regarded; it has turned out, however, that denser pipe separations did not lead to relevant increase of the thermal efficiency. The solutions 88-60-88 mm and 146-146 mm per fin thus were regarded as optimal designs under economic and constructive boundary conditions, prototyped and subsequently tested at ISFH; the related test method is explained in Section 3. The respective measurements are indicated by the red point in Figure 2(a). Referring to the case of 88-60-88 mm pipe separation, the data U_{int} = 56 W/(m^{2}K) measured with the prototype falls in the interval between the simulated data nodes $U_{int}(s_{eq}$ = 0,1 mm) = 48 W/(m^{2}K), and $U_{int}(s_{eq}$ = 0,01 mm).= 60 W/(m^{2}K). By linear extrapolation of the inverse function $s_{eq}(U_{int})$ we can identify a corresponding air gap width

$$s_{eq}\ (56\ \text{W/(m}^2\text{K)}) \approx 0{,}025\ \text{mm}$$

for the tested prototype. We see from the curvature of the simulated data in Figure 2(a), that further reduction of the gap widths s_{eq} has limited effect on the heat transfer coefficient U_{int} at this level. Therefore, cost-intensive measures to increase the manufacturing quality are not quite justified.

2.2 Hydraulic field modelling

The PV/T prototype design also regards hydraulic field simulations. Design target is an optimal (uniform) flow distribution of the fluid through the heat exchanger channels of the profile due to balanced hydraulic pressure resistances. The hydraulic pressure losses of the collector fields was evaluated by means of finite element methods for various flow settings and field geometries. Figure 3 shows the result - overall pressure loss and related thermal power - as function of the area-specific mass flow for a selected parallel hydraulic layout. Due to the hydraulic design of the collector components and the harp construction of the parallel heat exchangers, the collector field exhibits laminar and very uniformly distributed flow conditions within the heat exchanger profiles. Accordingly, the main hydraulic resistance is expected for the main connecting pipes, where turbulent flow states are observed even at very low mas flow rates. The simulations confirm this sensitivity, compare the blue lines in Figure 3 regarding two pipe diameters of 26 mm (solid line) and 32 mm (dashed line), respectively.

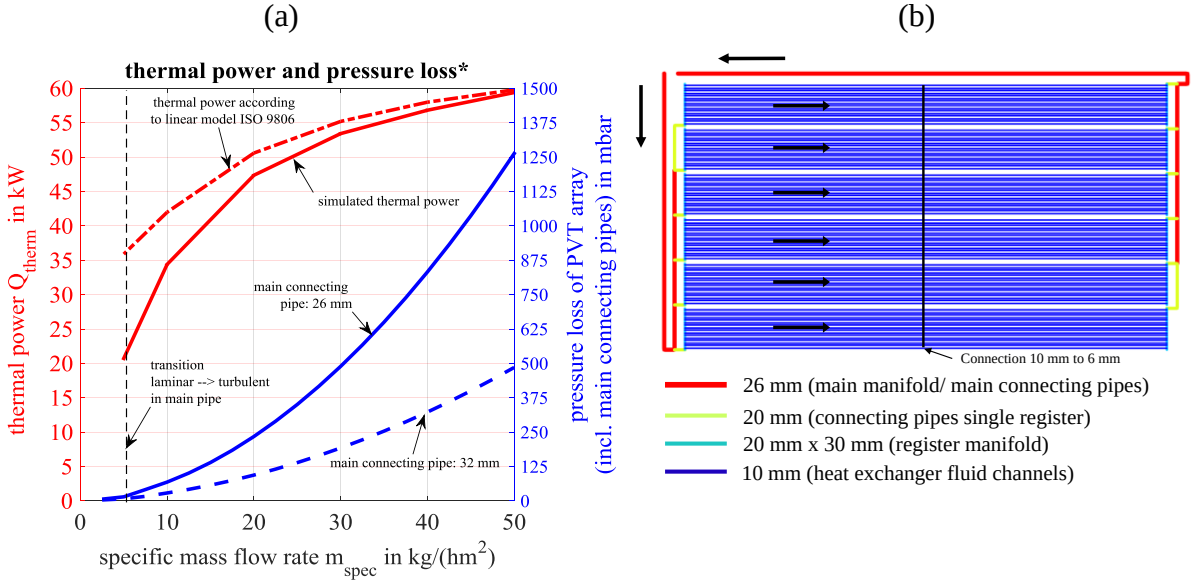

*conditions: T_a = 15 °C; T_{in} = 5 °C; wind 1.3 m/s; G''= 900 W/m^2; s_{eq} = 0,01 mm; tilt angle 38 °; 35 % ethylene glycol; Calyxo Module with 91 % absorption rate; Collector coefficients based on simulations in 2015 and operation in MPP

Figure 3: (a) Pressure drop simulation and related thermal power of a 14 x 7.2 m^2 PV/T field array shown in (b) with selected design pipe dimensions.

Figure 3 indicates that low specific mass flows well reduce the overall pressure losses at the expense of the

thermal performance (red lines). This is mainly due to an increase of the collector temperature and related heat losses as well as the nonlinear increase of temperature between inlet and outlet. Solid and dashed red lines refer to the FEM model and a linear model according to ISO 9806, respectively. The latter is included for comparison purposes. We see that the linear ISO 9806 model over-estimates the thermal power of the collector device for small flow rates in comparison to the FEM model. The following aspects are responsible for a significant decrease of the thermal power compared to the characteristics at reference value of 50 kg/(hm^2):

- ISO 9806 only regards the heat losses: lower mass flow rates lead to higher average collector temperatures
- ISO 9806 disregards flow-related changes of the internal convective heat transfer coefficient.
- ISO 9806 relays on linear temperature progressions between fluid in- and outlet; that assumption is only valid for higher mass flow rates.

The experimental tests and simulations have been carried out at 50 kg/(hm^2). At 10 kg/(hm^2), the thermal power is approximately 42 % lower than at the nominal design power, mostly due to the non-linear temperature increase and the higher collector temperature. Only 3 to 4 % of the thermal losses are due to less efficient convective heat transfer. Hence, The collector coefficients identified in standard thermal power tests lose their validity. The expected thermal power is 18 % lower than the calculating value according to ISO 9806. This aspect has a considerable practical relevance, because the mass flow rate of real systems is commonly adapted to the user´s demand and to the specific heat supply system, whereas the collector area is dimensioned to fulfil the minimum heat requirement in winter or just to fit the roof size.

3. Experimental performance assessment

3.1 Prototype test array

To assess the thermal efficiency of the system we installed a 20 m^2 prototype test field, as shown in Figure 4, and carried out long-term measurements. To reproduce realistic installation conditions, a wooden substructure was established which the PV/T array is mounted on. The test array consists of 24 thin-film CdTe modules of type Calyxo CX 3 75 W, of which three horizontal registers á 6 modules per string are used for the PV/T system. The PV/T system has a gross area of 14 m^2. To evaluate the mounting system and the architectural quality of the installation, a string of the left 6 modules is not thermally activated. Between PV generator and PV/T system, we placed dummy plates of black powder coated aluminium.

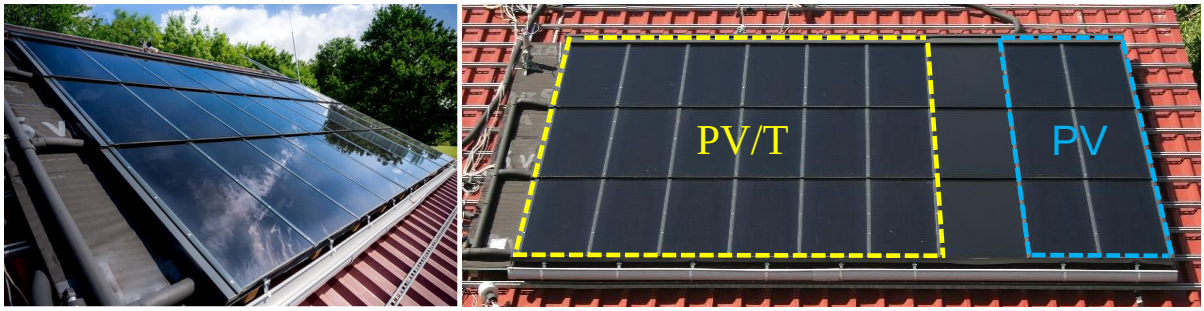

Figure 4: Roof-integrated PV/T prototype test field

The PV/T array is connected to a heat pump system and is operated with a 30% ethylene glycol mixture over a wide range of inlet temperatures from -10 °C to 60 °C. The system is equipped with an extensive system to evaluate the thermal performance according to the Standard ISO 9806, analyse the thermal behaviour of the components and record the electrical voltages and currents of the PV strings. The test facility enables to control inlet temperatures and fluid mass flows. The Maximum Power Point of the PV generator (the largest product of current and voltage) is achieved by using a conventional 2 kW inverter.

3.2 Quasi-dynamic performance tests

For the determination of the thermal collector coefficients according to ISO 9806: 2017 (ISO, 2017), we applied the quasi-dynamic method (QDT, quasi-dynamic testing). The QDT method is particularly suitable for the characterisation of so-called WISC (wind and infrared sensitive collectors) under fluctuating weather conditions. The standard also allows the determination of the thermal power $\dot{Q}_{th}$ of PV/T collectors, which for this reason have to be tested during operation in MPP. The most commonly used steady-state method (SST) requires very

stable weather conditions (i.e. clear sky). It gives no information about the heat capacity of the collector and tolerates low scatter of the measurement values. Furthermore, the angular dependence of the incident radiation (IAM, incident angle modifiers) must be determined by separate measurement, e.g. using a sun-tracking test device. However, the measurable collector area is also limited on tracking devices and small collector surfaces lead to high uncertainties concerning the reference surface and, thereby, the results for thermal efficiency. In the quasi-dynamic method, the influence of the incident angle is an integral part of the collector model and is determined from the same data set used to define all other collector efficiency parameters. This allows a comprehensive characterization of the stationary installed large test array.

The model equation to be used for determining the thermal power according to the QDT method incorporates (up to) 11 coefficients (ISO, 2017)

$$\begin{aligned}\dot{Q}_{\mathrm{th}}/A_{\mathrm{G}} = {} & \eta_{0,\mathrm{b}}\, K_{\mathrm{b}}(\Theta_{\mathrm{L}}, \Theta_{\mathrm{T}})\, G_{\mathrm{b}} + \eta_{0,\mathrm{b}}\, K_{\mathrm{d}}\, G_{\mathrm{d}} - a_1(\vartheta_{\mathrm{m}} - \vartheta_{\mathrm{a}}) - a_2(\vartheta_{\mathrm{m}} - \vartheta_{\mathrm{a}})^2 \\ & - a_3 u(\vartheta_{\mathrm{m}} - \vartheta_{\mathrm{a}}) + a_4(E_{\mathrm{L}} - \sigma T_{\mathrm{a}}^4) - a_5\, \mathrm{d}\vartheta_{\mathrm{m}}/\mathrm{d}t - a_6 u G_{\mathrm{hem}} \\ & - a_7 u(E_{\mathrm{L}} - \sigma T_{\mathrm{a}}^4) - a_8(\vartheta_{\mathrm{m}} - \vartheta_{\mathrm{a}})^4\end{aligned} \tag{2}$$

Note that the angle dependency K_{b} may be expressed by several coefficients depending on the model (ISO, 2017). The heat output $\dot{Q}_{\mathrm{th}}$ is referred to the gross area A_{G} or indicated as total module output. The parameters $\eta_{0,\mathrm{b}}$, K_{b}, K_{d} and $a_1 \ldots a_8$ are determined by fit to measured power data, $\dot{Q}_{\mathrm{th,m}}$. The coefficient a_8 is only relevant for concentrating collectors. The standard requires a replacement of the wind u by $u' = u - 3$ m/s for comparability with glazed flat-plate collectors, which is neglected here. The quasi-dynamic method was analysed in detail and the physical plausibility of the results was evaluated. We have optimized the calculation procedure, implemented it in the software *Matlab* and developed a new tool for parameter identification. The collector coefficients according to ISO 9806 are determined from the measured values by applying a multiple and robust least squares regression that uses the nonlinear mathematical identification method based on the *Matlab* function "nlinfit". The parameter a_4 represents the sky temperature dependence of the heat-loss coefficient and has a special meaning, since a standard-compliant parameter identification in many cases causes an (unwanted) neglect or miscalculation of the radiation exchange between sky and collector. This depends on correlations between the regressors of a_4, $\eta_{0,\mathrm{b}}$ and the IAM. For WISC collectors, such correlations lead to a statistically uncertain determination of the collector coefficients. To avoid this problem, we refer to the model for uncovered collectors under stationary conditions of ISO 9806: 2013 (ISO, 2013), the predecessor standard of ISO 9806: 2017 (ISO, 2017):

$$\frac{\dot{Q}_{\mathrm{th}}}{A_{\mathrm{G}}} = \eta_{0,\mathrm{hem}} \cdot G''(1 - b_{\mathrm{u}} \cdot u) - (b_1 + b_2 \cdot u)(\vartheta_{\mathrm{m}} - \vartheta_{\mathrm{a}}) \tag{3}$$

G'' takes into account the solar absorption coefficient α and the IR emission coefficient ε of the upper glass pane as well as the blackbody temperature of the atmosphere T_{sky}:

$$G'' = G + \frac{\varepsilon}{\alpha} \cdot \sigma \cdot \left(T_{\mathrm{sky}}^4 - T_{\mathrm{a}}^4\right) \tag{4}$$

The ratio ε/α is the decisive factor for the calculation of the coefficient a_4, which is to be determined by regression according to ISO 9806: 2017, but was presupposed as known in ISO 9806: 2013 before starting the parameter identification. For the hemispherical emissivity of PV glass, we assume ε = 0.84. For the absorption of the used CdTe modules a value of α = 0.91 was reported (Brötje et al., 2018). By comparison between Eq. (2) and (3) we obtain the following coefficients (see also ISO 9806: 2017):

$$a_1 = b_1 \tag{5}$$

$$a_3 = b_2 \tag{6}$$

$$a_4 = \eta_{0,\mathrm{hem}} \cdot \frac{\varepsilon}{\alpha} \tag{7}$$

$$a_6 = \eta_{0,\mathrm{hem}} \cdot b_{\mathrm{u}} \tag{8}$$

$$a_7 = \eta_{0,\mathrm{hem}} \cdot b_{\mathrm{u}} \cdot \frac{\varepsilon}{\alpha} \tag{9}$$

The nominal efficiency for hemispheric radiation is defined by the equation

$$\eta_{0,\mathrm{hem}} = \eta_{0,\mathrm{b}} \cdot K_{\mathrm{b}}(\Theta) \cdot \frac{G_{\mathrm{b}}}{G} + \eta_{0,\mathrm{b}} \cdot K_{\mathrm{d}} \cdot \frac{G_{\mathrm{d}}}{G} \tag{10}$$

Neglecting the non-significant coefficients, the final equation reads

$$\frac{\dot{Q}_{\mathrm{th}}}{A_{\mathrm{G}}} = \eta_{0,\mathrm{b}} \cdot K_{\mathrm{b}}(\Theta) \cdot G_{\mathrm{b}} + \eta_{0,\mathrm{b}} \cdot K_{\mathrm{d}} \cdot G_{\mathrm{d}} - a_1 \cdot (\vartheta_{\mathrm{m}} - \vartheta_{\mathrm{a}}) - a_2 \cdot (\vartheta_{\mathrm{m}} - \vartheta_{\mathrm{a}})^2$$
$$- a_3 \cdot u \cdot (\vartheta_{\mathrm{m}} - \vartheta_{\mathrm{a}}) + \eta_{0,\mathrm{hem}} \cdot \frac{\varepsilon}{\alpha} \sigma \cdot \left(T_{\mathrm{sky}}^4 - T_{\mathrm{a}}^4\right) - a_5 \cdot \frac{\mathrm{d}\vartheta_{\mathrm{m}}}{\mathrm{d}t} - \eta_{0,\mathrm{hem}} \cdot b_{\mathrm{u}} \cdot u \cdot G_{\mathrm{hem}} \quad (11)$$

For the definition of the coefficient $K_b(\theta)$, we implemented the interpolation point model by Isakson (1995), which is applicable to any solar thermal collector and allows to set any support angles for the interpolation depending on the needs and the actual curve of the angular dependence for the direct radiation. Disadvantages are the increased computational effort and an unstable regression in case of an unsuitable selection of the interpolation points. The approach is described in Eq. (12).

$$K_{\mathrm{b}}(\Theta_{\mathrm{j}}) = K_{\mathrm{b}}(\Theta_{\mathrm{i}}) + (\Theta_{\mathrm{j}} - \Theta_{\mathrm{i}}) \frac{K_{\mathrm{b}}(\Theta_{\mathrm{i}}) - K_{\mathrm{b}}(\Theta_{\mathrm{i+1}})}{\Theta_{\mathrm{i}} - \Theta_{\mathrm{i+1}}} \quad (12)$$

3.3 Measurements and data evaluation

Figure 5 shows the measured values used to determine the thermal collector coefficients in MPP mode according to the specifications from ISO 9806: 2017. The data was recorded every 10 seconds and averaged over 30 seconds for our evaluation. The specific mass flow of the heat carrier was set to 50 kg/(hm^2).

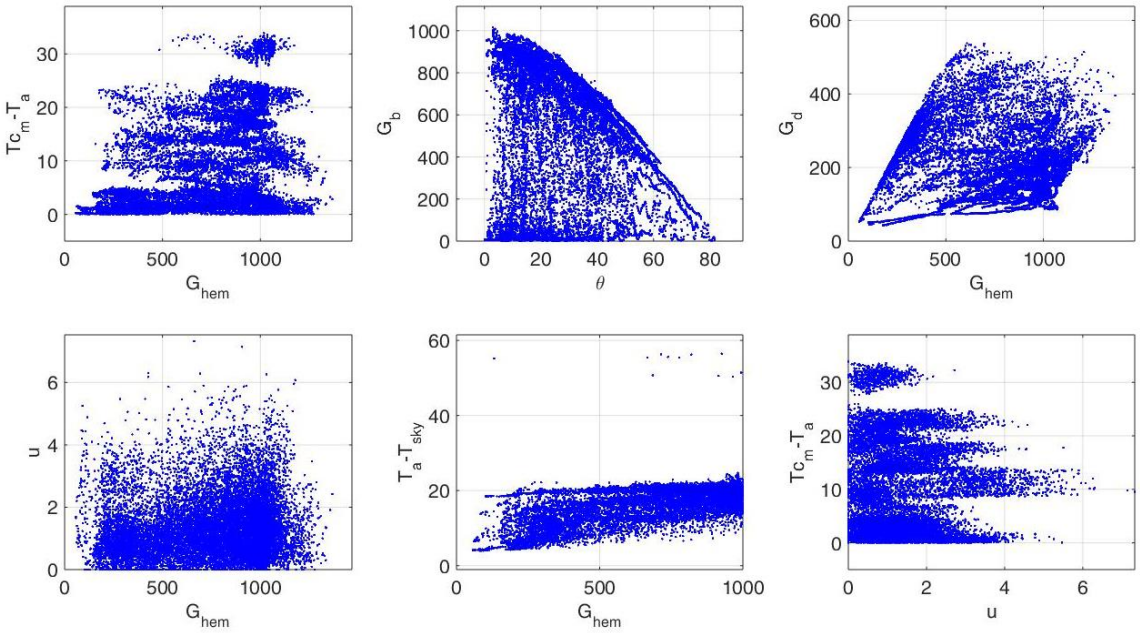

Figure 5: Measurement data filtered according to ISO 9806: 2017 (operated in MPP, march to June 2017)

An iterative procedure was used to determine the parameters of the collector, in order to avoid disturbing influences due to correlations. Each iteration consists of two steps:

1. From the measured values which have already been filtered according to ISO 9806: 2017, only those operating points that fulfil the temperature and incident angle conditions -1,0 K < $\vartheta_{\mathrm{m}} - \vartheta_{\mathrm{a}}$ < +1,0 K and -10 ° < Θ < 10 ° are considered in the first step. The intervals of $\vartheta_{\mathrm{m}} - \vartheta_{\mathrm{a}}$ and Θ depend on the available measurement data and on the collector type. They must be carefully selected and, if possible, adjusted to achieve convergence in the regressions. The result is a set of strictly selected data, which is used to identify $\eta_{0,\mathrm{b}}$ of equation (11). The parameters $K_b(\theta)$ to a_6 are set as constant start values during this procedure.
2. In a second iteration step, the parameters $K_b(\theta)$ to a_6 are determined from the complete data set according to the requirements of ISO 9806. During this procedure, the parameter $\eta_{0,\mathrm{b}}$, is set to the constant value determined in step 1. Using the new set of coefficients, we iterate the procedure until the convergence criteria are matched (such as $\Delta_i(x)$ < 0.01 % for each parameter).

The convergence of the parameter identification procedure is very good for the investigated prototype because of the large amount and variation of test data. Tables 1 to 3 show the characteristics of the installed PV/T collector

prototype according to the modified power equation model (11). The coefficients were converted according to the equations (5) to (9). The T-ratio is a measure of the statistical certainty of each coefficient and is formed from the numerical value and the standard deviation σ of the specific coefficient. A high T-ratio means a safe mathematical regression, but not necessarily a physical correlation as expected in the model. According to ISO 9806, T > 3 is required, but T > 10 was observed to be a more reliable limit. Absolute uncertainties, if mentioned, refer to the 95% confidence level.

3.4 Operation in maximum power point (MPP) of PV generator

Table 1 features the results of the parameter identification for the prototype test array in MPP mode. A strong convergence with $\Delta_i(x) < 0.01$ % was achieved after 18 iterations. The support angles selected for the calculation of the IAM were 50 °, 65 ° and 80 °.

Table 1: Thermal coefficients of the investigated PV/T test array in MPP mode

Coefficient	Value	Dimension	$T = x/\sigma$	Coefficient	Value	Dimension	$T = x/\sigma$
$\eta_{0,b}$	0.658 ±0.018	-	329	a_2	0.09	W/(m^{2}K^2)	18
$K_b(50°)$	0.92	-	219	a_3	1.26	J/(m^{3}K)	24
$K_b(65°)$	0.90	-	51	a_4 (ε/α)	0.61 (0.92)	-	(fixed)
$K_b(80°)$	0.85	-	7	a_5	47.00	kJ/(m^{2}K)	179
K_d	0.99	-	198	a_6	0.03	s/m	44
a_1	11.56	W/(m^{2}K)	69				

3.5 Converting coefficients from MPP to OC mode

The electrical efficiency of the CdTe modules under STC conditions is η_{el} = 10.4 % according to the product data sheet. As shown in Figure 6, the electrical efficiency of the DC side of the PV generator at a calculated cell temperature of 25 ° C is approximately 9.9 %. The measured efficiency scatter is quite large; therefore, thus inducing a wide uncertainty range of η_{el}.

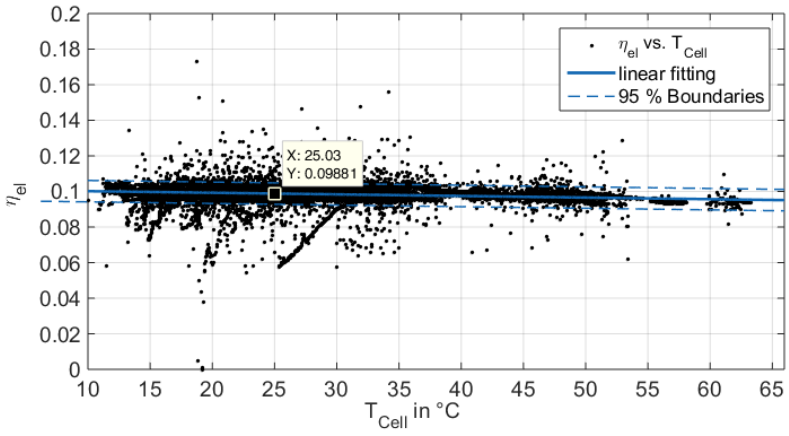

Figure 6: Electrical efficiency of the investigated PV/T test array operating in MPP

By regression of the electrical efficiency data we determined a temperature-power coefficient of Y = - 0.21 %/K (data sheet: - 0.25 %/K). Some part of the energy is dissipated by radiation and thus it is not available for conversion into sensible heat. Neglecting the low temperature dependence of electrical output of the CdTe modules, we can estimate the thermal zero-loss efficiency in OC mode based on the value measured in MPP mode. Assuming a single node or capacity for the collector, the efficiency in OC mode can be calculated from equation (13).

$$\eta_{0,OC} \approx \frac{\eta_{0,MPP}}{1 - \eta_{el,STC}/\alpha} \tag{13}$$

Using η_{el} = 10.4 % and the measured absorption α = 0.91, we determine a thermal efficiency $\eta_{0,OC}$ = 0.743. The collector coefficients in OC operation mode are of interest because collector models used in simulation tools like *TRNSYS* or *Polysun* require them (Vela Solaris AG, 2018; Stegmann et al., 2011). The input data must be supplemented by the characteristics of the PV modules. The heat resistance between PV cells and heat carrier is only considered by *TRNSYS* through the internal heat transfer coefficient U_{int}.

The electric current I_{el} and the voltage U_{el} of the PV modules were additionally recorded during the measurement. Using this information, we can compare the thermal coefficients in MPP and in OC mode more comprehensively. In order to determine the OC characteristics of the PV/T collector by means of multiple regression, we modify the regression model according to Eq. (11). The area-related electrical power results from

$$p_{el} = \sum_{String\ 1-3} (U_{el} \cdot I_{el}) / 13.6\ m^2 \quad (14)$$

We assume that the conversion of solar radiation into electricity is equivalent to a reduction of the available direct and diffuse radiation and that both radiation components generate the PV power with the same efficiency. The corrected irradiation data are calculated by using equations (15) and (16). We replace G_b and G_d in equation (11) and obtain the collector coefficients shown in table 2. Taking into account the uncertainties of $\eta_{0,b}$(OC) and $\eta_{0,b}$(MPP) of 2 percentage points each in the MPP mode, the result show a good agreement with the value estimated according to equation (13).

$$G'_b = G_b \cdot \left(1 - \frac{p_{el}}{G \cdot \alpha_{eff}}\right) \quad (15)$$

$$G'_d = G_d \cdot \left(1 - \frac{p_{el}}{G \cdot \alpha_{eff}}\right) \quad (16)$$

Table 2: Thermal PV/T collector coefficients (OC mode) converted from the characteristics in MPP mode

Coefficient	Value	Dimension	$T = x/\sigma$	Coefficient	Value	Dimension	$T = x/\sigma$
$\eta_{0,b}$	0.748 ±0.019	-	323	a_2	0.13	W/(m^{2}K^2)	25
$K_b(50°)$	0.93	-	232	a_3	1.32	J/(m^{3}K)	25
$K_b(65°)$	0.91	-	52	a_4 (ε/α)	0.61 (0.92)	-	(fixed)
$K_b(80°)$	0.86	-	16	a_5	48.38	kJ/(m^{2}K)	187
K_d	0.97	-	204	a_6	0.03	s/m	46
a_1	10.90	W/(m^{2}K)	69				

3.6 Operation in open circuit (OC) of PV generator

To determine the thermal characteristics for the actual operation of the PV/T test array without electricity, the PV strings were separated from the inverter. Table 3 reports the collector coefficients determined on the basis of measurement data recorded in April 2018.

Table 3: Thermal PV/T collector coefficients as determined from measurements in OC mode

Coefficient	Value	Dimension	$T = x/\sigma$	Coefficient	Value	Dimension	$T = x/\sigma$
$\eta_{0,b}$	0.743 ±0.016	-	217	a_2	0.11	W/(m^{2}K^2)	9
$K_b(50°)$	0.98	-	268	a_3	1.18	J/(m^{3}K)	12
$K_b(65°)$	0.97	-	85	a_4 (ε/α)	0.61 (0.92)	-	(fixed)
$K_b(80°)$	0.45	-	7	a_5	37.03	kJ/(m^{2}K)	85
K_d	0.93	-	110	a_6	0.02	s/m	25
a_1	11.24	W/(m^{2}K)	43				

Even in this case, taking into consideration the uncertainties of $\eta_{0,b}$(OC) and $\eta_{0,b}$(MPP), the experimental result is in very good agreement with the value determined according to equation (13). The comparison between tables 2 and 3 shows that the MPP measurements can also be used for a first estimation of the performance of the collector in electrical open circuit (OC). The power curves in OC mode basically result from a parallel shift of the power curves in MPP, as represented in Figure 7. The heat capacity a_5 and the incident angle modifiers are the coefficients which most significantly differ in the two operation modes.

The heat capacity a_5 is an effective, physically simplified quantity and is strongly influenced by the thermal resistance between the PV module and the fluid, the fluid mass flow and the time interval considered in the parameter identification. These influences depend on the use of the single-node model in ISO 9806, which does not take into account transient heat conduction between absorbing material and fluid. The capacity measured in OC mode is supposed to be smaller than in MPP mode because electricity generation is a temporal damper for temperature changes in the collector. The conversion into electrical exergy takes place immediately and significantly faster than the heat transfer processes.

3.7 Thermal power curves

Figure 7 shows the performance characteristics of the PV/T prototype for standard reporting conditions according to ISO 9806: 2017 (see Table 4).

Table 4: Standard reporting conditions (SRC) according to ISO 9806:2017

Weather conditions	**Blue sky**	**Hazy sky**	**Grey sky**
Direct radiation G_b	850 W/m^2	440 W/m^2	200 W/m^2
Diffuse radiation G_d	150 W/m^2	260 W/m^2	200 W/m^2
Ambient temperature T_a	20 °C	20 °C	20 °C
Wind speed u in m/s	1,3	1,3	1,3
Incident angle modifier K_b	1	1	1
Thermal radiation $\sigma \cdot (T_{sky}^4 - T_a^4)$	- 100 W/m^2	- 50 W/m^2	0 W/m^2

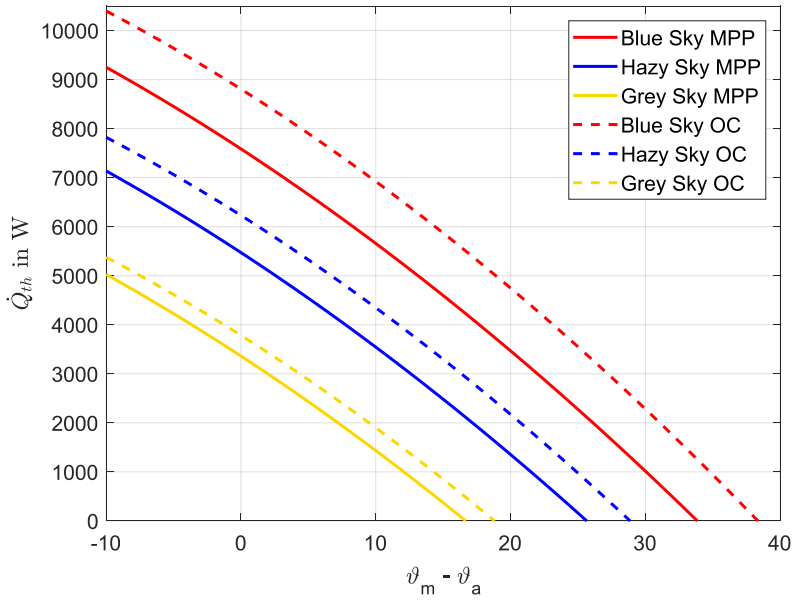

Figure 7: Thermal performance of the developed PV/T at Standard Reporting Conditions based on PV/T gross area 13.6 m^2

The curves represent the total thermal power with refer to the thermally activated collector area for MPP and OC operation based on the efficiency parameters from tables 1 and 3. The peak power is calculated according to the Standard for the total area of 13.6 m^2 under blue sky conditions, $\vartheta_m - \vartheta_a = 0$ K and u = 1.3 m/s. $\dot{Q}_{peak,MPP} = 7586 \pm 232$ W in MPP and $\dot{Q}_{peak,OC} = 8806 \pm 329$ W in OC. The correspondent area-related thermal output is $\dot{q}_{peak,MPP} = 558 \pm 17$ W/m^2 and $\dot{q}_{peak,OC} = 647 \pm 24$ W/m^2. The standard uncertainties for peak power are 3.1 and 3.7 percentage points respectively. The stagnation temperature is defined at $\dot{Q}$ = 0 W, u = 0 m/s, 30 ° C ambient temperature and blue sky. It amounts to 69 °C in MPP and 73 °C in OC.

3.8 Internal heat transfer coefficient

Using eq. (5), (6) and (8) as well as the thermal coefficients from the parameter identification, we can estimate the internal heat transfer coefficient U_{int} of the new prototype according to Stegmann et al. (2011) by use of equation (17).

$$U_{int} = \frac{\alpha_{eff} \cdot (a_1 + a_3 \cdot u)}{\alpha_{eff} - \eta_{0,hem} + a_6 \cdot u} \qquad (17)$$

The coefficient a2 is not taken into account in this approach because it is referred to ISO 9806:2013. Repeating the parameter identification by neglecting a_2, we obtain a 95 % confidence interval U_{int} = 47 ... 68 W/(m^{2}K) at a wind speed of 1.3 m/s. Although the collector coefficients are determined with high accuracy, the confidence interval of U_{int} is quite large. Table 5 sums up the confidence intervals of U_{int} and of each coefficient, respectively. The results show that the internal heat transfer coefficient is almost unaffected by the wind speed. All results refer to OC operation.

Table 5: Confidence interval of the internal heat transfer coefficient U_{int} for different wind speeds and of the collector efficiency parameters

Parameter	95 % confidence interval		Value
	lower limit	upper limit	
α_{eff}	0.91		0.91
$\eta_{0,b}$	0.73	0.76	0.74
K_d	0.90	0.95	0.92
a_1	10.35	12.14	11.20
a_3	0.85	1.51	1.18
a_6	0.03	0.03	0.03
U_{int} at 0 m/s	48.3	70.6	57.0
U_{int} at 1.3 m/s	**47.3**	**68.0**	**55.9**
U_{int} at 3 m/s	46.4	65.7	54.8

The experimentally determined value U_{int} = 55.9 W/(m^{2}K) is marked in Figure 2 to quantitatively evaluate the thermal contact between the PV module and the heat exchanger of the prototype. The comparison with the simulation indicates an equivalent air gap clearly smaller than 0.1 mm. Considering the uncertainties in the determination of U_{int}, the upper limit of the confidence interval of is above technically plausible values. The lower limit of U_{int} = 47.3 W/(m^{2}K) means a still very small average air gap of about 0.1 mm. That result indicates that there is not much potential for performance improvements at this point, since even a perfect connection would improve $\eta_{0,hem}$ by approximately +0.01 (see Figure 2). As already mentioned in Section 2, s_{eq} is an effective value, resulting from both directly contacted areas and areas with air gaps > 0.1 mm.

4. Simulations of thermal power under non-standard conditions

In addition to the determination of the characteristic values of the PV/T system under standard conditions, the qualitative behavior under extreme conditions such as negative power (cooling case) and condensation was investigated. Figure 8 displays examples of the measured and calculated area-specific thermal power under different operating and ambient conditions during MPP operation of the PV generator.

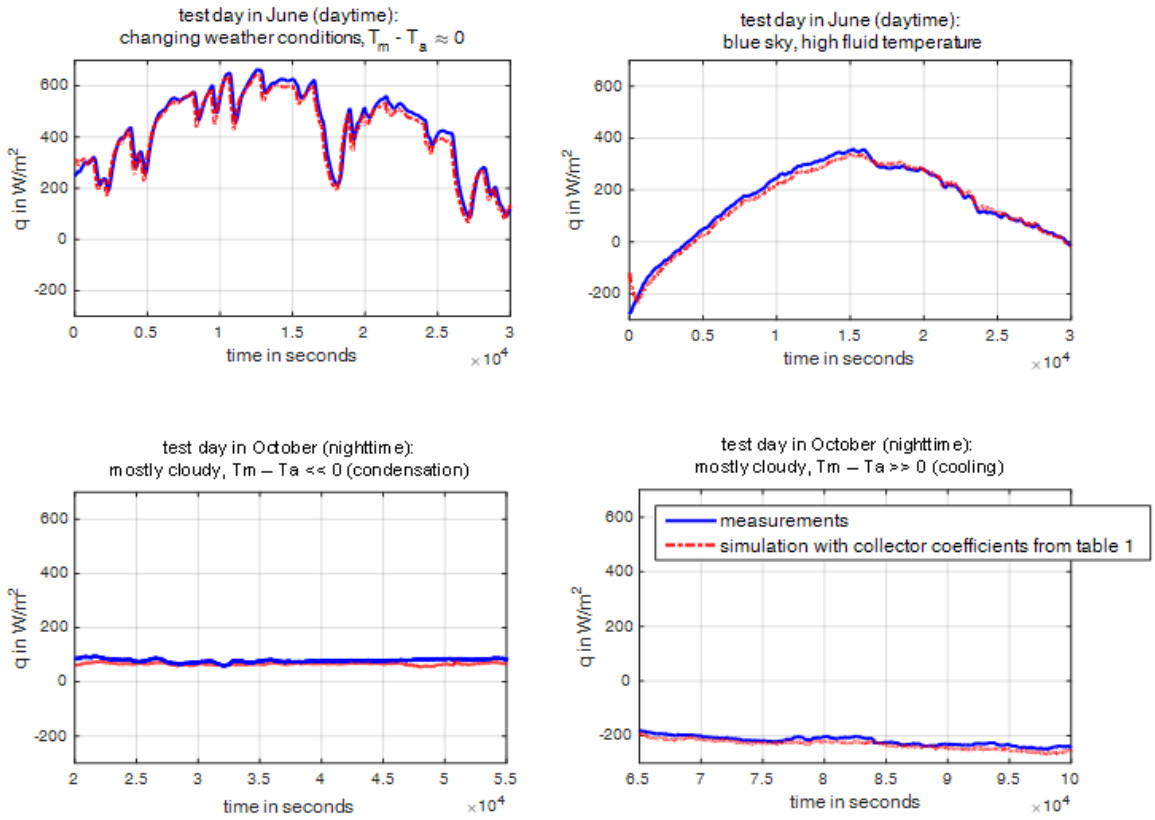

Figure 8: Measured and modeled thermal power output of the investigated prototype PV/T roof (CET: central European time)

For the calculation of the simulated power, the QDT collector model according to ISO 9806: 2017 was implemented in *Matlab Simulink* (version R2015a). Thereby, the change of the mean collector temperature is calculated by solving the correspondent differential equation (2), as in the simulation models of e.g. *Polysun* or *TRNSYS*. Using the measured temporal change of the mean collector temperature dTm/dt would lead to a high level of fluctuation in the simulations, which makes it difficult to evaluate the accuracy of the identified coefficients for the prediction of thermal performance based on weather data.

The comparisons between simulations and measurements show that the determined collector coefficients and the model can reproduce the thermal behavior of the collector with a good accuracy even under conditions that deviate from the measurement conditions used for the parameter identification.

Heat from condensation is predominantly gained at night and can contribute to the thermal yield of uncovered collectors, especially in winter, at low irradiation levels. Operating the collector prototype at low temperatures confirmed the occurrence of condensation. During the investigation period we couldn't collect enough data for a final evaluation of possible heat gains.

5. Conclusions

The newly developed PV/T system for roof integration with a glue-free connection between the PV module and the heat exchanger ensures a nearly optimal heat transfer into the fluid due to its robust construction and low manufacturing tolerances, which provide for a very small air gap. Compared to the preliminary system, the zero-loss efficiency could be increased from 44 % to 74 % (OC mode) thanks to the improved design. The efficiency is quite high, also in comparison with other PV/T collectors on market. The modular roof-integrated system features high architectural quality and allows a high flexibility for the application in the building sector. Several public and private pilot projects are about to be implemented.

The quasi-dynamic test method was successfully applied. In order to avoid mathematical correlation problems, the data evaluation was implemented with modified steps. The thermal collector coefficients in OC mode, required for heat transfer evaluation and system simulations, can be calculated from measured data obtained in MPP mode by using simple equations. Therefore, performance tests in OC mode are assessed as non-mandatory for the presented type of collector. This approach has to be tested for different types of PV/T collectors.

6. Acknowledgements

This publication is based on the project "ModulTech – Solarhybrid", which is funded by the German Federal Ministry for Economic Affairs and Energy on the basis of a decision of the German Federal Parliament (16KN041920). The authors are grateful for the financial support. The authors thank the project partners, Carsten Grobe Passivhaus and blue energy systems GmbH, for the cooperation. We would like to thank the technicians Ralf Hartmann and Henri Dieckmann for their support and Prof. Dr.-Ing. Oliver Kastner for proofreading. The content of this publication is in the responsibility of the authors.

References

Incropera, F.P., DeWitt, D.P., 2002. Fundamentals of heat and mass transfer, 5th ed. Wiley, New York.

ISO, 2013. ISO 9806:2013 - Solar energy - Solar thermal collectors - Test methods.

ISO, 2017. ISO 9806:2017 - Solar energy - Solar thermal collectors - Test methods.

Stegmann, M., Bertram, E., Rockendorf, G., 2011. Model of an unglazed photovoltaic thermal collector based on standard test procedures. Proceedings of 30th ISES Solar World Congress, Kassel, Germany 2011. DOI:10.18086/swc.2011.19.30.

Brötje, S., Kirchner, M., Giovannetti, F., 2018. Performance and heat transfer analysis of uncovered photovoltaic-thermal collectors with detachable compound. Solar Energy 170, 406–418. DOI:10.1016/j.solener.2018.05.030.

Vela Solaris AG, 2018. Polysun software. Https://frontstore.velasolaris.com/wordpress/ (last access: 24.11.2018).

Isakson, P., 1995. Solar Collector Model for Testing and Simulation. Final Report for BFR project Nr. 900280-1, Building Services Engineering, Royal Institute of Technology.